Behavioral stochastic resonance: How a noisy army betrays its outpost

Jan A. Freund, Jochen Kienert, and Lutz Schimansky-Geier
Institut für Physik, Humboldt-Universität zu Berlin, Invalidenstrasse 110, D-10115 Berlin, Germany

Beatrix Beisner
Center for Limnology, University of Wisconsin-Madison, Madison, Wisconsin 53706

Alexander Neiman, David F. Russell, Tatyana Yakusheva, and Frank Moss
Center for Neurodynamics, University of Missouri at St. Louis, St. Louis, Missouri 63121
(Received 20 August 2000; published 27 February 2001)

Juvenile paddlefish prey upon single zooplankton by detecting a weak electric signature resulting from its feeding and swimming motions. Moreover, it has recently been shown that paddlefish make use of stochastic resonance near the threshold for prey detection: a process termed behavioral stochastic resonance. But this process depends upon an external source of electric noise. A swarm of plankton, for example, *Daphnia*, can provide this noise. Assuming that juvenile paddlefish attack single *Daphnia* as outliers in the vicinity of the swarm, making use of noise from the swarm, we calculate the spatial distribution of the average phase locking period for the subthreshold signals acting at the paddlefish rostrum. Numeric evaluation of analytic formulas supports the notion of a noise-induced widening of the capture area quantitatively.

DOI: 10.1103/PhysRevE.63.031910 PACS number(s): 87.19.Dd, 05.40.−a, 87.17.Nn, 87.50.−a

I. INTRODUCTION

We have recently shown that juvenile paddlefish, *Polyodon Spathula*, make use of stochastic resonance (SR) in the detection and capture of planktonic prey at the threshold of their perception [1]. Prey are detected, tracked, and located exclusively by means of an elaborate array of electroreceptors spread over the animal's rostrum, or paddle shaped nose-like appendage. *Polyodon Spathula* is a primitive creature whose fossil record extends into the Cretaceous period (65 million years ago) [2]. This, together with some recent physiological evidence [3], suggests that behavioral SR is an evolved survival strategy. The paddlefish, which is found only in the river basins of the Midwestern United States and in the Yangtze River in China, feeds exclusively on zooplankton. Moreover, paddlefish are largely bottom feeders where the light is poor and where, in turbulent, silt-laden waters, vision is limited. In order to survive in this environment, they have evolved the aforementioned electrosensory system. Juvenile paddlefish (less than one year old) locate, track, and feed on single plankton [4], whereas older fish, after having developed gill rakers, filter feed on swarms.

The *Daphnia*, a plankton of 1 to 2 mm in length commonly found in North American fresh water, is a favorite food of the paddlefish. *Daphnia* emit weak dipole-shaped electric signals with both oscillatory (4–8 Hz) and dc components. Though the dc component is much larger, we here study only detection of the ac component by means of stochastic synchronization. Due to the dipole-like shape of the field, the intensity of a *Daphnia* signal at the fish's rostrum is expected to drop off rapidly with distance. Indeed, it has recently been shown, using the dipole characteristic $1/r^3$ drop-off, that the capture probability with distance exhibited by the fish mimics the Fisher information on its rostrum from a single *Daphnia* [5]. *Daphnia* that appear at a larger distance from the fish's rostrum are less likely to be detected and/or captured. But weak signals from distant single *Daphnia* can be enhanced, and consequently the probability that they are captured, by an external noise source [1]. In Ref. [1], we applied a uniform electric noise field parallel to the rostrum in order to demonstrate behavioral SR. Here we investigate the possibility, already suggested in Ref. [1], that a swarm of *Daphnia* can provide the necessary source of external noise in the wild. Thus the noise from an army of *Daphnia* can help to reveal the locations of its outposts.

SR has its roots in notions about global climate dynamics put forth in the early 1980s [6]. A large interest in SR has arisen, especially since its introduction into experimental sensory biology [7] and its observation in membrane ion channels [8]. It has been the subject of a report [9] and several reviews [10]. In the simplest view, called threshold, or nondynamical SR [11], only three ingredients are necessary: a threshold, a subthreshold signal, and noise. Originally, however, SR was described as noise-induced switching of the state point in a bistable potential [12], and this is the view we take here. Indeed, in the original biological application of SR, the information contained in the barrier crossings of the state point in a weakly, periodically modulated bistable potential provided the first quantitative explanation of the famous phase locking phenomenon widely observed in sensory biology [13]. Example data from the auditory nerve fibers of the squirrel monkey and from the visual cortex of the cat were presented in support of that explanation.

We consider an outlier *Daphnia* in the vicinity of the swarm as the source of a weak periodic signal. The signal from this single *Daphnia* is detected at the rostrum of a paddlefish. The swarm is assumed to be spherical with diameter $\Lambda = 100$ cm. In the reference frames of the single *Daphnia* and the center of the swarm, the two vectors $\vec{\mathbf{r}}$ and $\vec{\mathbf{R}}$ represent the distances to the paddlefish rostrum, respectively. For a schematic setup of this scenario see Fig. 1.

At the rostrum, noise from the swarm is added to the

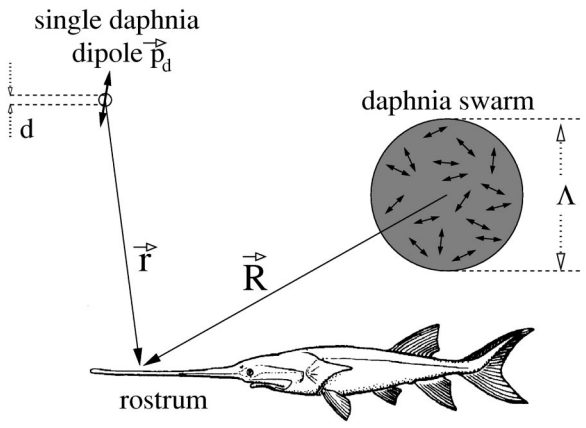

FIG. 1. The setup of the predator-prey-noise system. The *Daphnia* swarm which is assumed to be spherical provides the noise background. The geometry is specified by the two distance vectors $\vec{\mathbf{r}}$ and $\vec{\mathbf{R}}$, the extension of a single *Daphnia d*, and the diameter of the *Daphnia* swarm Λ. The single *Daphnia* dipole is indicated by a little arrow.

weak signal from the single *Daphnia*. The detecting unit switches stochastically between two states, with transition rates governed by both the signal amplitude A and the noise intensity D experienced at the detector site. Recently, the phenomenon of SR was linked to the effect of noise-induced phase synchronization [14]: for optimal noise the average duration of locking episodes can increase enormously [15]. Stochastic synchronization has already been experimentally demonstrated in the paddlefish electroreceptor system where for weak stimuli it is a possible encoding scheme [16]. Applied to our case this means we can explore the beneficial role of swarm noise by analyzing the average number of periods the fish can receive before a phase slip disturbs the signal detection.

We emphasize that the averaging implied above need not be temporal, but instead almost certainly is an ensemble average over a population of thousands of receptor cells. In this case the synchronization of the array of receptors over one or a few cycles of the signal amounts to an encoding based on timing precision. A form of SR based on a measure of spike timing precision has recently been demonstrated for a parallel array of Hodgkin–Huxley-type receptors with summed outputs [17], a type of connectivity thought to be common in sensory biology. The array can achieve a high degree of synchronized timing precision upon application of a single, subthreshold stimulus pulse [17]. Synchronization of the array response during only one or even a fraction of a single cycle of the applied stimulus is therefore possible via this mechanism. However, for an ergodic system, as assumed here, temporal averaging is equivalent. Moreover, if one receptor cell can synchronize with the external field, it has been shown that under the same conditions all others can also [18]. It is therefore sufficient to study a temporal average over many signal cycles applied to a single receptor. Owing to the dependence of A and D on the geometry, i.e., the positions of swarm (center), single *Daphnia*, and the rostrum (detector), we compute the spatial distribution of the average duration of locking episodes $\langle T_{\mathrm{lock}} \rangle$ and normalize it to the signal period, thus yielding $\langle n_{\mathrm{lock}} \rangle = \Omega \langle T_{\mathrm{lock}} \rangle / 2\pi$. We emphasize that our synchronization approach is nonlinear in nature. The nonlinearity of the synchronization theory [14,15] is necessary in order to account for the dependence of the output on signal amplitude or distance to the *Daphnia*.

In Sec. II we briefly describe the swarming behavior of *Daphnia* populations and outline some current ideas regarding their interactions with one another. In Sec. III we display the characteristics of the signal from a single *Daphnia* and the noise from a *Daphnia* swarm. We then outline in Sec. IV the theory of effective phase locking and show how $\langle n_{\mathrm{lock}} \rangle$ is calculated from knowledge of the average frequency $\langle \dot{\varphi} \rangle$ and effective diffusion coefficient $\mathcal{D}$ of a phase difference φ. In a twice dichotomic signal description $\langle \dot{\varphi} \rangle$ and $\mathcal{D}$ can be expressed via two rates a_1 and a_2 (Sec. V) which, in turn, are determined by the signal amplitude A and the noise intensity D. The dependence of A and D on geometrical distances is derived in Sec. VI. In Sec. VII we apply these calculations to the detection problem faced by a juvenile paddlefish seeking to capture a single *Daphnia* in the vicinity of the swarm. Contours of constant $\langle n_{\mathrm{lock}} \rangle$ in the neighborhood of the swarm delineate optimal tracking and capture strategies for juvenile feeding. Our predictions appear to be experimentally testable. Finally, a summary and an outlook are given in Sec. VIII.

II. DAPHNIA SWARMS

Daphnia are the most commonly studied freshwater zooplankton, in large part because they are widely distributed, abundant, and easily sampled and cultured. *Daphnia* inhabit the pelagic (open-water) zones of lakes and slow-moving rivers and are very important prey for fish. They are cyclic parthenogens, that is they spend the greater part of the growing season reproducing clonally. No actual mating needs to occur for reproduction, and consequently individuals do not need to find each other. Thus there is no reproductive advantage (in terms of finding mates) to swarming. *Daphnia* swim with a hopping motion induced by a powerful downbeat of the modified second antenna followed by a brief period of sinking. They can modify their swimming pattern (turning frequency) and swim speed depending on several factors including food density [19], predators [20], and light intensity [21].

Several studies have noted the tendency of *Daphnia* individuals to swarm or display a clumped spatial distribution [22,23]. These swarms consist of very high-density aggregations, with 1000–9000 individuals per liter observed. Individuals may use photons emitted by other individuals to recognize each other and determine interneighbor distances in the swarms [24]. Several hypotheses have been proposed to explain swarming behavior in *Daphnia*. Swarming for mating purposes [22] and the avoidance of predation are the two major explanations [23,25]. Because swarms often consist of parthenogenetic individuals, the mating hypothesis can be excluded in most cases. Other swarm characteristics lend credence to the predator-avoidance hypothesis. Swarming more often occurs during daylight hours than at night

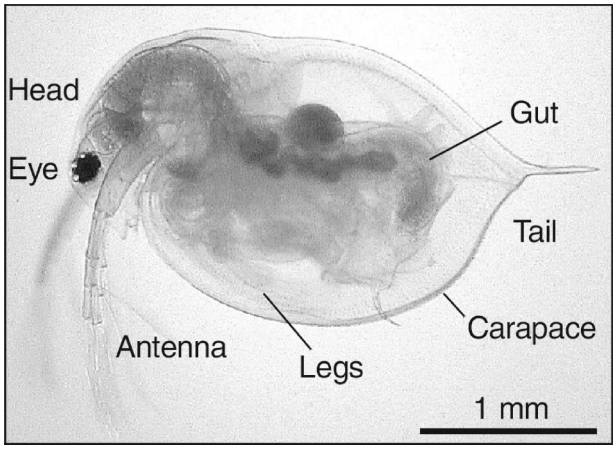

FIG. 2. The single *Daphnia*.

[23,26]. When in a swarm, the swimming speed of all individuals is remarkably uniform, though they move and hop in random directions, and much slower than when they are solitary (e.g., speed of 2 mm/s within swarms versus 7 mm/s as solitaries) [20].

There is also a tendency of individuals to circle inwards and downwards in the swarms [27]. Probably the strongest evidence for swarming being induced by predation arises from studies of trace chemicals exuded by predators [20,28]. These chemical compounds, which act as cues, can be from fish, invertebrate predators or even from the crushed bodies of *Daphnia* themselves. The tendency of a population of *Daphnia* to respond to predator exuded chemicals may depend on their previous exposure to such a predator [28]. These results suggest that for most swarms formed during the growing season, the most likely explanation is the avoidance of predation by visual predators (generally vertebrates like planktivorous fish or by invertebrate like *Chaoborus sp.*) [19,20,23]. The tendency to form groups benefits a single individual, because the movement of many identical individuals can distract predators and decrease their attack rates. In addition, for each individual, there is a dilution effect afforded by being within a group when faced with a predator. Swarming in *Daphnia* is likely a permanent behavioral strategy in systems where predators are abundant [20].

III. SIGNAL AND NOISE CHARACTERISTICS

The signal from a single *Daphnia* and noise from the swarm can be measured. A single *Daphnia* is shown in Fig. 2.

Figure 3 shows the time course of the potential measured at a distance of 1.2 mm behind the abdomen.

The potential consists of both ac and dc components, but here we concentrate on the ac, or oscillatory, component. Recent experiments have shown that the behavioral responses, scored as strikes, exhibit a bandpass characteristic with a maximum response between 5 and 15 Hz. Responses were less frequent at higher (20, 40, and 50 Hz) and lower (0.1, 0.5, and 1 Hz) test frequencies, with a steep drop-off below 5 Hz [29]. The shape of the potential at distances of 1

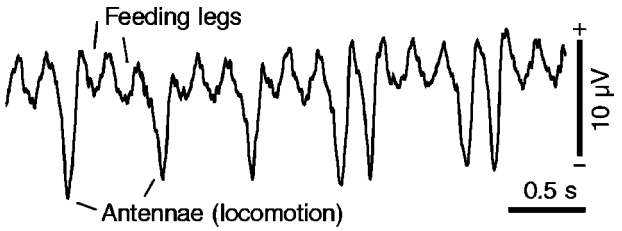

FIG. 3. Electric oscillations from a tethered *Daphnia* can be correlated with rhythmic beating of the feeding legs or antennae.

cm or more is approximately a dipole, and in this work we shall assume it to be a dipole.

The power spectrum of the experimental *Daphnia* signal is shown in Fig. 4

There are two main frequency components, a broader one around 5 Hz, which results from feeding motions of the appendages, and a narrower one at about 7 Hz resulting from swimming motions. Note that both these oscillatory components are superimposed on a broad noise background. For the sake of simplicity we shall omit the swimming frequency and concentrate on the 5 Hz feeding frequency.

In Fig. 5(A) we show the photograph of a swarm in an aquarium together with the experimental setup (electrodes, isolation, etc.). Figures 5(B)–(D) show the time course of the noise voltage (B) measured at the recording electrode (*el*), together with its related power spectrum (C), and amplitude distribution (D). We note that the amplitude distribution is well approximated by a Gaussian as shown by the solid curve. The power spectrum is approximately a Lorentzian related to Ornstein-Uhlenbeck noise [30] which itself is generated from

$$\ddot{\xi}+\left(\frac{1}{\tau_1}+\frac{1}{\tau_2}\right)\dot{\xi}+\frac{1}{\tau_1\tau_2}\xi(t)=\sqrt{\frac{D}{\tau_1\tau_2}}\Gamma(t), \qquad (1)$$

where Γ is Gaussian white noise (Wiener process), i.e.,

$$\langle\Gamma(t)\rangle=0 \quad \text{and} \quad \langle\Gamma(t)\Gamma(t')\rangle=2\delta(t-t'), \qquad (2)$$

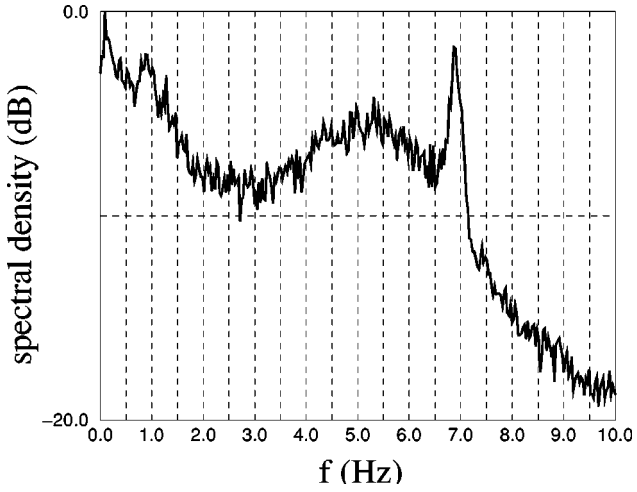

FIG. 4. The power spectrum of the experimental single *Daphnia* signal.

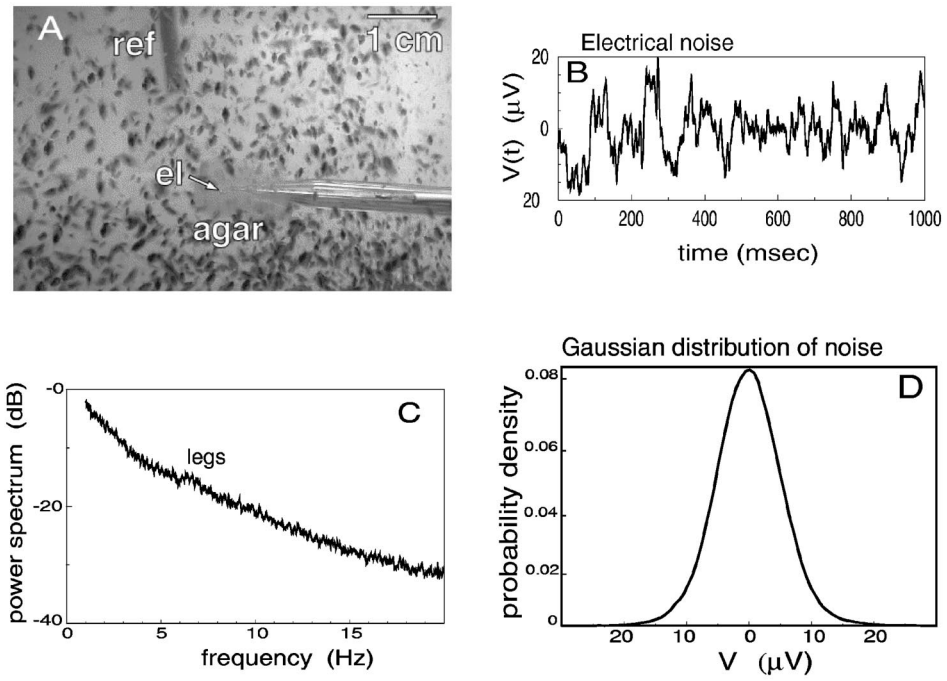

FIG. 5. A: A photograph of a *Daphnia* swarm with *ref* denoting the reference and *el* the recording electrode, respectively. The arrow points to the 1 mm diameter silver ball and *agar* is the *agarus* isolation preventing direct contact of *Daphnia* with the recording electrode. B: A fragment of the voltage record. The time series was filtered using a high-pass filter at 0.5 Hz. C: Power spectrum of the recorded swarm voltage. D: The voltage probability distribution extracted from the recorded swarm signal exhibits a Gaussian shape.

and D controls the intensity of fluctuations. The left-hand side of Eq. (1) establishes a second order low-pass filter. The constants τ_1 and τ_2 have the meaning of two correlation times, as can be read from the stationary correlation function (assuming $\tau_1 > \tau_2$)

$$C(\tau) = \frac{D}{\tau_1^2 - \tau_2^2}\left[\tau_1 \exp\left(-\frac{|\tau|}{\tau_1}\right) - \tau_2 \exp\left(-\frac{|\tau|}{\tau_2}\right)\right]. \quad (3)$$

The analytic expression for the power spectrum reads

$$S_{\xi\xi}(\omega) = \frac{2D}{[1-\tau_1\tau_2\omega^2]^2 + [\tau_1+\tau_2]^2\omega^2}. \quad (4)$$

In the context of swarm noise the parameters τ_1 and τ_2 characterize the fictitious dynamics of a stochastic electric source which emits the swarm signal. The case $\tau_2 \ll \tau_1$ corresponds to the common overdamped limit of the Ornstein–Uhlenbeck process. Later, we need threshold crossing rates for the sum of a sinusoidal signal $A\sin(\Omega t)$ and colored Gaussian noise $\xi(t)$. For these rates to remain finite the spectral density has to decay with at least the fourth power of the frequency [31], hence, both τ_1 and τ_2 should be nonvanishing.

In Fig. 6 we fitted Eq. (4) to the measured spectrum [Fig. 5(C)].

The best fit of Eq. (4) to the experimental data yields $\tau_1 = 0.13$ s and $\tau_2 = 0.017$ s which means that an oscillator generating such a spectrum is far from being overdamped; the swarm signal is closer to so-called harmonic noise [32].

IV. SIGNAL DETECTION AND PHASE LOCKING

The classical evaluation of SR with periodic signals proceeds by computing the spectral power amplification (SPA) or the signal-to-noise ratio (SNR) [10]. Here, we will use an alternative approach which employs the concept of phase locking.

Since we are interested in a noise-induced phenomenon we have to treat the stochastic generalization of classic phase locking [33]. The introduction of noise requires one to reconsider the phase locked situation, originally meaning that the difference between an input and an output signal remains constant, in terms of finite locking periods which are interrupted and separated by short phase slips. When the average length of locking episodes assumes values which are large compared to the signal period it is reasonable to speak about effective phase synchronization.

These statements are made precise by derivation of a dynamic equation for the phase difference $\varphi = \phi_{\text{out}} - \phi_{\text{in}}$ which is known as the Adler equation [34]

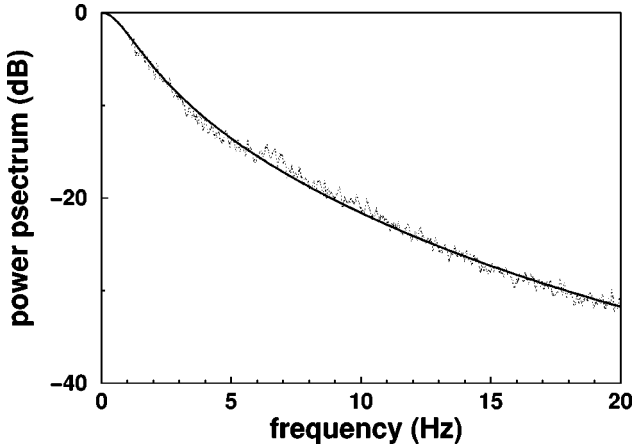

FIG. 6. The experimental power spectrum from Fig. 5 C (dotted line) and Eq. (4) with constants $\tau_1 = 0.13$ s and $\tau_2 = 0.017$ s (solid line). Note that due to the normalization of the experimental spectrum the noise intensity D is still undetermined.

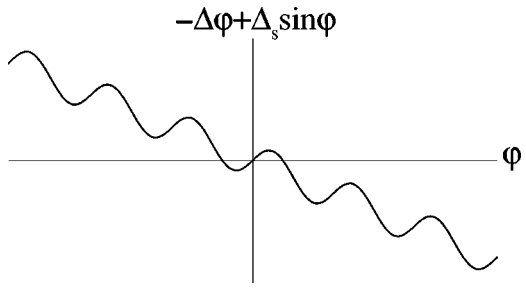

FIG. 7. The stochastic dynamics of the phase difference φ can be understood as the motion of a fictitious Brownian particle in an undulated and tilted potential.

$$\dot{\varphi} = \Delta - \Delta_s \cos\varphi + \xi. \tag{5}$$

In the framework of stochastic processes one can interpret this dynamics as the motion of a fictitious Brownian particle which moves in a corrugated and inclined potential landscape [cf. Fig. 7].

Here Δ is the so-called frequency mismatch, i.e., the difference between the natural oscillator frequency Ω_0 and the input frequency $\Omega_{\rm in}$. Δ_s is the synchronization bandwidth. The latter term becomes clear when realizing that a locking episode means that the particle wiggles around inside one of the wells while a noise-induced jump to a neighboring well corresponds to a phase slip. As can be seen from Eq. (5), the potential possesses wells only if $|\Delta| < \Delta_s$; this necessary condition for phase synchronization says that the system generating the output can synchronize only with input signals whose detuning is less than Δ_s.

For the case that Δ and Δ_s are independent from the noise intensity, fluctuations $\xi(t)$ can only deteriorate the mechanism of phase synchronization. The awesome constructive role fluctuations play in SR has its counterpart in the phenomenon of noise-induced phase coherence [35]: now both Δ and Δ_s are not only functions of the signal amplitude A but also of the noise intensity D.

The average duration of locking episodes can be computed from an ansatz for the mean square displacement

$$\langle \varphi^2 \rangle = \langle \dot{\varphi} \rangle^2 \langle T_{\rm lock} \rangle^2 + 2\mathcal{D} \langle T_{\rm lock} \rangle = \pi^2. \tag{6}$$

Average growth of φ^2 is decomposed in a drift and a diffusive component. In the next section we will briefly review how the average frequency $\langle \dot{\varphi} \rangle$ and the phase diffusion coefficient $\mathcal{D}$, not to be mixed with the noise intensity D, can be derived analytically in the framework of a fully dichotomic signal description. Then it will also become clear why we define a phase slip by the distance π.

From Eq. (6) we can readily write down an expression for the mean number of signal periods experienced during an average locking episode

$$\langle n_{\rm lock} \rangle = \frac{\langle T_{\rm lock} \rangle}{T_{\rm in}} = \frac{\Omega_{\rm in}}{2\pi} \frac{\mathcal{D}}{\langle \dot{\varphi} \rangle^2} \left[\sqrt{1 + \left(\frac{\pi \langle \dot{\varphi} \rangle}{\mathcal{D}} \right)^2} - 1 \right]. \tag{7}$$

The limiting cases for the drift and the diffusion dominated regimes read for $\mathcal{D} \ll \pi |\langle \dot{\varphi} \rangle|$:

$$\langle n_{\rm lock} \rangle = \frac{\Omega_{\rm in}}{2\pi} \frac{\pi}{|\langle \dot{\varphi} \rangle|} \left[1 - \frac{\mathcal{D}}{\pi |\langle \dot{\varphi} \rangle|} + \frac{1}{2} \left(\frac{\mathcal{D}}{\pi \langle \dot{\varphi} \rangle} \right)^2 + \cdots \right] \tag{8}$$

for $\mathcal{D} \gg \pi |\langle \dot{\varphi} \rangle|$:

$$\langle n_{\rm lock} \rangle = \frac{\Omega_{\rm in}}{2\pi} \frac{\pi^2}{2\mathcal{D}} \left[1 - \frac{1}{4} \left(\frac{\pi \langle \dot{\varphi} \rangle}{\mathcal{D}} \right)^2 + \cdots \right]. \tag{9}$$

The phenomenon of noise-enhanced signal detection shows up by a dramatic increase of the quantity $\langle n_{\rm lock} \rangle$: under conditions of sufficiently large, albeit subthreshold signal amplitude and optimal noise, the paddlefish detects many periodic beats of the single *Daphnia*. In the context of our geometric setup [cf. Fig. 1] the efficiency of detection will vary from place to place. Hence we will plot the spatial distribution of the quantity $\langle n_{\rm lock} \rangle$ to substantiate our central thesis.

V. DICHOTOMIC SIGNAL DESCRIPTION

To derive how $\langle \dot{\varphi} \rangle$ and $\mathcal{D}$ depend on A and D we specify a dichotomic description of both the output $y(t)$ and input $x(t)$ signals. The two states between which the signals switch back and forth are chosen as -1 and $+1$ and can be connected to the instantaneous phases $\phi_{\rm out}$ and $\phi_{\rm in}$ via

$$y(t) = \exp[i\phi_{\rm out}(t)] = \exp[ik_{\rm out}(t)\pi], \tag{10}$$

$$x(t) = \exp[i\phi_{\rm in}(t)] = \exp[ik_{\rm in}(t)\pi]. \tag{11}$$

$k_{\rm out}(t)$ and $k_{\rm in}(t)$ are point processes describing the related switching events and simply accumulate the number of switches which occurred up to time t since initialization. Hence by construction the phases are discontinuously increasing functions of time. Following from its definition, the phase difference $\varphi = \phi_{\rm out} - \phi_{\rm in}$ is also restricted to multiples of π but increases or decreases discontinuously depending on whether the output or the input is jumping.

The stochastic dynamics of the phase difference $\varphi(t) = k(t)\pi$ is specified by fixing the transition rates between the four states shown in Fig. 8.

Switches of the input occur regularly at all integer halves of the input signal, i.e., the periodic process is not stationary but only cyclostationary

$$\hat{\Omega}(t, \vartheta) = \pi \sum_{n=-\infty}^{\infty} \delta\left(t - \frac{n\pi + \vartheta}{\Omega} \right), \tag{12}$$

where ϑ is some initial phase. To achieve stationary statistics we have to perform a subsequent averaging with respect to ϑ

$$\langle \hat{\Omega} \rangle_\vartheta = \int_0^{2\pi} \hat{\Omega}(t, \vartheta) \frac{d\vartheta}{2\pi} = \Omega. \tag{13}$$

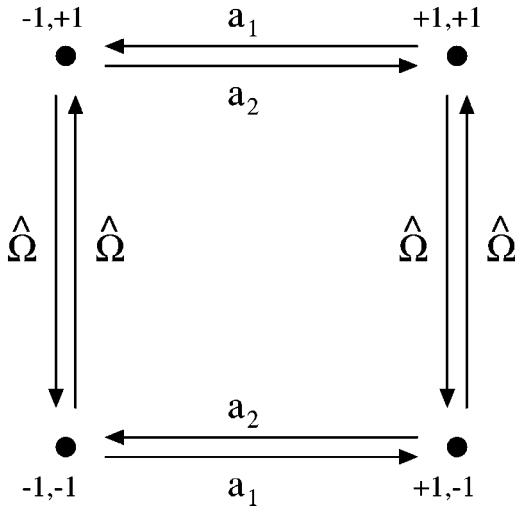

FIG. 8. The twice dichotomic description defines the 2×2-state system: horizontal transitions describe a switch of the output while vertical ones correspond to switches of the input. The synchronous states, i.e., $+1,+1$ and $-1,-1$, are favored by the condition $a_1 \leqslant a_2$ (for further explanations see text).

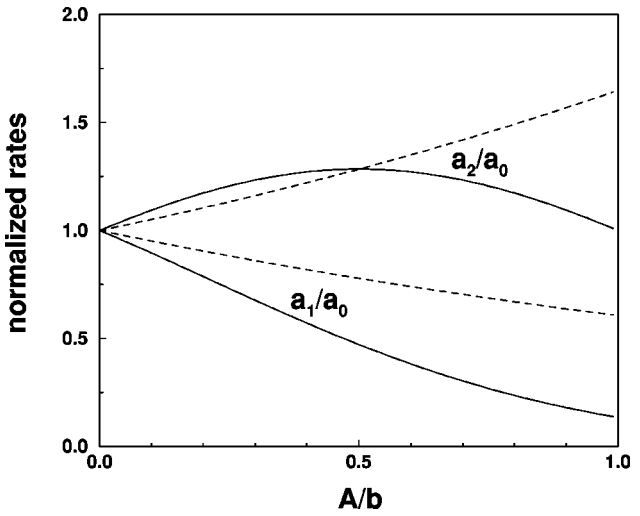

FIG. 9. In contrast to the standard Kramers' rates $a_{1/2} = a_0(\bar{\sigma}, \tau_1, \tau_2)\exp(\mp\bar{A}/2\bar{\sigma^2})$ (dashed) the expressions used in Eqs. (16) and (17) (solid lines) are not monotonously diverging with increasing signal amplitude; all curves for $\bar{\sigma}=1$.

The rates a_1 and a_2, governing switchings of the output, are modeled such that they favor the synchronous states $(+1, +1$ and $-1,-1)$ above the asynchronous ones $(+1,-1$ and $-1,+1)$. To achieve this we have to obey $a_1(A,D) \leqslant a_2(A,D)$.

The time modulated threshold crossing rates $r_{cr}(t)$ for the sum of a sinusoidal signal $A\sin(\Omega t)$ and colored Gaussian noise [cf. Eq. (1)] were computed in [36]

$$r_{cr}(t) = \frac{1}{2\pi\sqrt{\tau_1\tau_2}}\exp\left(-\frac{[1-\bar{A}\sin(\Omega t)]^2}{2\bar{\sigma^2}}\right) \times\left[\exp\left(-\frac{\bar{A}^2}{2\bar{\sigma^2}}\right)+\frac{1}{2}\bar{A}\epsilon\sqrt{\frac{2\pi}{\bar{\sigma^2}}}\cos(\Omega t) \times\mathrm{erfc}\left(-\frac{\bar{A}\epsilon\cos(\Omega t)}{\sqrt{2\bar{\sigma^2}}}\right)\right] \quad (14)$$

with dimensionless scaled parameters

$$\bar{A}=\frac{A}{b}, \quad \bar{\sigma^2}=\frac{D}{b^2(\tau_1+\tau_2)}, \quad \epsilon=\sqrt{\Omega^2\tau_1\tau_2}, \quad (15)$$

where D, τ_1, and τ_2 are as in Eq. (1) and b denotes the threshold. Note that subthreshold signals correspond to the range $0<\bar{A}<1$.

Since our theoretical approach used both dichotomic output and input, the latter justified by, say, some preprocessing of the continuous sinusoidal signal, we can identify the rates a_1 and a_2 with

$$a_1=\frac{1}{2\pi\sqrt{\tau_1\tau_2}}\exp\left(-\frac{1}{2\bar{\sigma^2}}\right)\exp\left(-\frac{\bar{A}(1+\bar{A})}{\bar{\sigma^2}}\right), \quad (16)$$

$$a_2=\frac{1}{2\pi\sqrt{\tau_1\tau_2}}\exp\left(-\frac{1}{2\bar{\sigma^2}}\right)\exp\left(+\frac{\bar{A}(1-\bar{A})}{\bar{\sigma^2}}\right). \quad (17)$$

The common prefactor of both rates $a_0(\bar{\sigma}, \tau_1, \tau_2)$ is independent of the normalized signal amplitude $\bar{A}$. The amplitude dependence in the exponent is nonstandard since it involves a square, diminishing both rates for large amplitude signals. Hence the maximum discrepancy between a_1 and a_2 does not occur for $\bar{A}=1$ as is the case for Kramers-like rates [cf. Fig. 9].

With the rates given by Eqs. (12) and (16) and (17) we can write down the master equation governing the probabilistic evolution of the phase difference φ

$$\frac{\partial P_k(t)}{\partial t}=\hat{\Omega}(P_{k+1}-P_k)+g_{k-1}P_{k-1}-g_kP_k, \quad (18)$$

where we have denoted $P_k=\mathrm{prob}(\varphi=k\pi)$ and $g_k=a_1$ for k even and $g_k=a_2$ for k odd. From there it is straightforward to calculate

$$\langle\dot{\varphi}\rangle=-\Omega+\frac{\pi}{2}(a_1+a_2)-\frac{\pi}{2}(a_2-a_1)\langle\cos\varphi\rangle. \quad (19)$$

Note that Eq. (19) is the analog to the averaged Adler equation (5) when identifying

$$\Delta=\frac{\pi}{2}(a_1+a_2)-\Omega \quad \text{and} \quad \Delta_s=\frac{\pi}{2}(a_2-a_1). \quad (20)$$

Note also that via a_1 and a_2 now both Δ and Δ_s are noise dependent. The quantity $\langle\cos\varphi\rangle$ turns out to be the input–output correlator [37]. Its asymptotic value can be computed yielding

$$\lim_{t\to\infty}\langle\cos\varphi\rangle=\langle\sigma^*\rangle=\frac{a_2-a_1}{2(\Omega/\pi)+(a_1+a_2)}, \tag{21}$$

hence it is also completely determined by the rates.

The phase diffusion coefficient $\mathcal{D}$ is defined by the relation

$$\mathcal{D}=\frac{1}{2}\partial_t[\langle\varphi^2\rangle-\langle\varphi\rangle^2]. \tag{22}$$

In principle, its computation from the master equation (18) is straightforward [38]; some subtle difficulties for strictly periodic input signals have been discussed in [15]. The result reads

$$\mathcal{D}=\frac{\pi^2}{2}\left[\frac{a_1+a_2}{2}+\left(\frac{\Omega}{\pi}-(a_2-a_1)\right)\langle\sigma^*\rangle - \left(2\frac{\Omega}{\pi}-(a_1+a_2)\right)\langle\sigma^*\rangle^2-\frac{a_2-a_1}{2}\langle\sigma^*\rangle^3\right]. \tag{23}$$

In Fig. 10 (top and bottom) we present double logarithmic plots of the average output frequency $\Omega+\langle\dot{\varphi}\rangle$ (normalized to Ω) and of the phase diffusion coefficient $\mathcal{D}$ (normalized to $\pi^2/2$), both as functions of the ''natural'' detector frequency $\Omega_0=\Omega+\Delta$ (normalized to Ω) for various normalized signal amplitudes $\bar{A}=0,0.1,\ldots,0.5$.

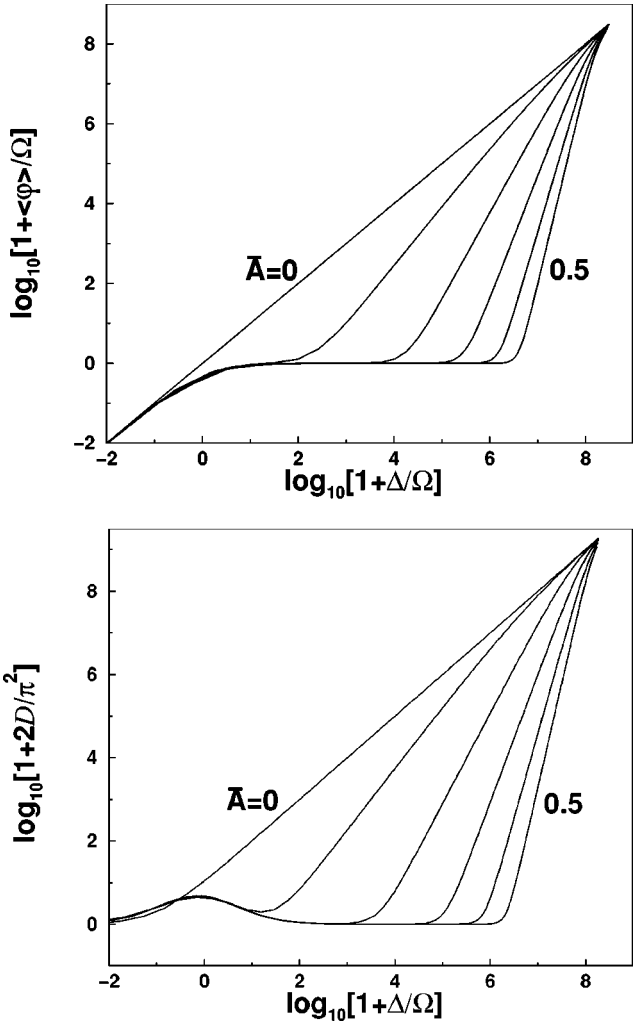

FIG. 10. The frequency and phase locking regions appear in these plots as plateaus around zero of the ordinate. The width of the plateau grows with increasing amplitude $\bar{A}=0,0.1,\ldots,0.5$. The tips in the upper right correspond to $\bar{\sigma}\to\infty$ where maximum flipping rate of the detector, given by $[2\pi\sqrt{\tau_1\tau_2}]^{-1}$, is experienced.

VI. GEOMETRIC DEPENDENCE OF *A* AND *D*

Inserting the expressions for $\langle\dot{\varphi}\rangle$ and $\mathcal{D}$ into Eq. (7), and by virtue of Eqs. (16) and (17) for the rates a_1 and a_2, we can compute $\langle n_{\rm lock}\rangle$, i.e., the average number of periods the fish can detect before a phase slip occurs, for given $\Omega,\bar{A},\bar{\sigma^2}$. What remains is to express (rescaled) signal amplitude and (rescaled) noise intensity as functions of the distances r and R, respectively [cf. Fig. 1].

As said before, the electric field of a single *Daphnia* is assumed to be a dipole field. As is known from classical electrodynamics, one has to distinguish between different regimes:

$$\text{near-field limit} \quad d\ll r\ll\lambda,$$

$$\text{intermediate region} \quad d\ll r\sim\lambda,$$

$$\text{far-field limit} \quad d\ll\lambda\ll r,$$

where d, λ, and r denote the extension of the dipole, the wavelength of the radiated ac field, and the distance between the dipole and the observation point, respectively. In our case d, the *Daphnia* size, is of the order of a few millimeters and the wavelength λ (for an oscillation of 5–10 Hz) far beyond the scale of a kilometer, hence, the near-field limit applies. In this limit the electric dipole field reads

$$\vec{E}(\vec{r})\sim\frac{3\vec{n}(\vec{n}\cdot\vec{p}_d)-\vec{p}_d}{r^3} \tag{24}$$

$$\sim\frac{p_d}{r^3}(\vec{n}2\cos\Theta-\vec{a}\cos\Phi\sin\Theta-\vec{b}\sin\Phi\cos\Theta), \tag{25}$$

where $\vec{p}_d$ is the dipole moment of the *Daphnia* and $\vec{a}$, $\vec{b}$, and $\vec{n}$ constitute a right-handed orthonormal basis. With $\vec{n}$ playing the role of the z axis, the *Daphnia* dipole moment can be represented in spherical coordinates, i.e., $\vec{p}_d=(p_d,\Phi,\Theta)$, cf. Fig. 11.

Considering only the field component along $\vec{n}$ we find the following result for the signal amplitude

$$A\sim\frac{p_d}{r^3}\cos(\Theta) \tag{26}$$

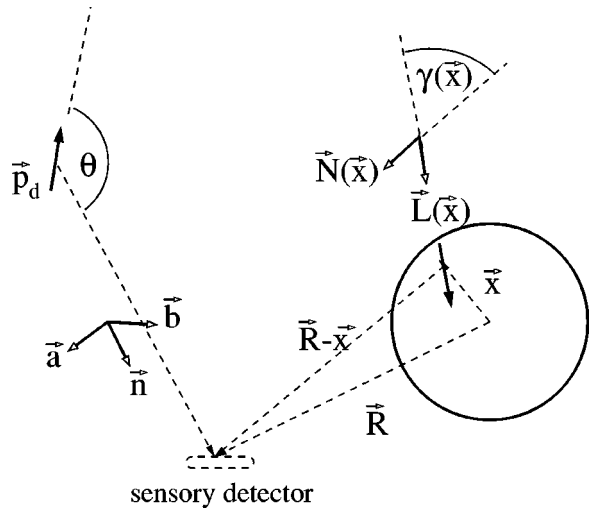

FIG. 11. The geometrical configuration illustrating our notation used in the derivations (see text).

which incorporates two important features: The dropping of the amplitude with respect to the distance according to a r^{-3} law, and the fact that the amplitude also depends on the *Daphnia* orientation: For $\theta=0$ or $\theta=\pi$ (emitting in the direction parallel to $\vec{r}$) the fish detects the *Daphnia* best[1] whereas for $\theta=\pi/2$ (emitting in the direction perpendicular to $\vec{r}$) the *Daphnia* is somewhat ''invisible.''

In what follows we will only consider the best case, i.e., we write

$$A=C_1\frac{1}{r^3}, \tag{27}$$

where the proportionality constant C_1 is achieved by a fit to the measured pair ($r=2.5$ cm, $A=1$ μV) yielding

$$C_1=\frac{125}{8}\mu\mathrm{V\,cm}^3. \tag{28}$$

To derive how the noise intensity D depends on the geometry we employ a continuum approach to model the *Daphnia* swarm. In the reference frame of the geometrical center of the *Daphnia* cloud [cf. Fig. 11] we describe the distribution of the population by the density $\rho(\vec{x})$. It is normalized to the total number N of *Daphnia*

$$\int \rho(\vec{x})d^3x=N. \tag{29}$$

Since we restrict ourselves to spherical distributions, i.e., $\rho(\vec{x})=\rho(x)$, the center of mass coincides with the geometrical center

$$\int \vec{x}\rho(x)d^3x=\vec{0}. \tag{30}$$

In accordance with the above near-field limit (24) the total electric field at the detector site (i.e., at the point $\vec{R}$) reads [cf. Fig. 11]

$$\vec{E}(\vec{R},t)\sim\int\frac{3\vec{N}(\vec{x})(\vec{N}(\vec{x})\cdot\vec{p}(\vec{x},t))-\vec{p}(\vec{x},t)}{|\vec{R}-\vec{x}|^3}\rho(x)d^3x+\text{c.c.} \tag{31}$$

with

$$\vec{N}(\vec{x})=\frac{\vec{R}-\vec{x}}{|\vec{R}-\vec{x}|} \tag{32}$$

and

$$\vec{p}(\vec{x},t)=p_d\vec{L}(\vec{x})e^{i[\omega(\vec{x})t-\psi(\vec{x})]}. \tag{33}$$

The unit vector $\vec{L}(\vec{x})$ accounts for the local orientation of the (net)dipole moment of *Daphnia* in a little cube centered around $\vec{x}$. Assuming the local orientations $\vec{L}(\vec{x})$, frequencies $\omega(\vec{x})$ and phases $\psi(\vec{x})$ to be independent random numbers corresponds to the assumption of incoherent activity of *Daphnia* in the swarm.

Then, the correlation function is proportional to

$$\begin{aligned}\langle\vec{E}(\vec{R},t)\cdot\vec{E}^*(\vec{R},t')\rangle\sim p_d^2\int\int d^3x\,d^3x'\frac{\rho(x)}{|\vec{R}-\vec{x}|^3}\frac{\rho(x')}{|\vec{R}-\vec{x}'|^3}\\ \times\langle[3\vec{N}(\vec{x})(\vec{N}(\vec{x})\cdot\vec{L}(\vec{x}))-\vec{L}(\vec{x})]\\ \cdot[3\vec{N}(\vec{x}')(\vec{N}(\vec{x}')\cdot\vec{L}(\vec{x}'))-\vec{L}(\vec{x}')]\rangle\\ \times\langle e^{i[\omega(\vec{x})t-\omega(\vec{x}')t']}\rangle\langle e^{-i[\psi(\vec{x})-\psi(\vec{x}')]}\rangle.\end{aligned} \tag{34}$$

Due to the random phase assumption the related term in brackets will only survive in case $\Delta\psi=0$, however, this means only for $\vec{x}=\vec{x}'$. Hence

$$\langle e^{-i[\psi(\vec{x})-\psi(\vec{x}')]}\rho(x')\rangle\to\delta(\vec{x}-\vec{x}'). \tag{35}$$

The first exponential in brackets in Eq. (34) will generate the basic structure of the Ornstein-Uhlenbeck (OU) spectrum [cf. Eq. (4)]

$$\langle e^{i[\omega(\vec{x})(t-t')]}\rangle\to\frac{1}{[1-\tau_1\tau_2\omega^2]^2+[\tau_1+\tau_2]^2\omega^2} \tag{36}$$

from which we conclude that

$$D\sim p_d^2\int\frac{\rho(x)}{|\vec{R}-\vec{x}|^6}\langle 3(\vec{N}(\vec{x})\cdot\vec{L}(\vec{x}))^2+\vec{L}^2(\vec{x})\rangle d^3x \tag{37}$$

[1]The transition from θ to $\theta-\pi$ simply corresponds to a signal which is phase shifted by π

$$\sim p_d^2 \int \frac{\rho(x)}{|\vec{R}-\vec{x}|^6} \langle 3\cos^2\gamma(\vec{x})+1\rangle d^3x, \tag{38}$$

where $\gamma(\vec{x})$ is the angle between the unit vectors $\vec{N}(\vec{x})$ and $\vec{L}(\vec{x})$ [cf. Fig. 11]. Assuming this local angle to be equidistributed over the range $[0,2\pi]$ and performing the average yields a factor 5/2.

The remaining integral

$$D \sim p_d^2 \int \frac{\rho(x)}{|\vec{R}-\vec{x}|^6} d^3x \tag{39}$$

can be evaluated in spherical coordinates and, assuming *Daphnia* to be equidistributed inside the swarm, i.e., $\rho(x) = N[\frac{4}{3}\pi(\Lambda/2)^3]^{-1}$, yields

$$D = C_2 \frac{N}{R^6} \frac{1}{\left(1-\frac{\Lambda/2}{R}\right)^3 \left(1+\frac{\Lambda/2}{R}\right)^3}, \tag{40}$$

where C_2 is a related proportionality constant. We note that for $R \to \Lambda/2$ (from above) a third order pole $(R-\Lambda/2)^{-3}$ in the intensity shows up due to the fact that the detector collects signal power from *Daphnia* in the immediate vicinity of the projected contact point; of course, when approaching the swarm too close, i.e., $(R-\Lambda/2) \sim \mathcal{O}(d)$, the dipole approximation of the electric field loses significance.

In the other extreme, $\Lambda/2 \ll R$, a rapid decrease according to an R^{-6} law indicates that the extension of the *Daphnia* cloud becomes unimportant. Due to the used near-field limit we also have to obey $R \ll \lambda$; however, this upper bound is practically irrelevant because at and beyond this point the intensity is negligible anyway.

Again, the proportionality constant C_2 occurring in Eq. (40) can be fixed by comparison with experimental data [1]. Thus for $D=1$ $(\mu\mathrm{V})^2$ Hz^{-1}, $\Lambda/2=2$ cm, $R=3$ cm, and $N=200$ we find

$$C_2 = \frac{5}{8} (\mu\mathrm{V})^2\,\mathrm{Hz}^{-1}\,\mathrm{cm}^6. \tag{41}$$

Being furnished with formulas (28) and (41) we have to determine $\overline{A}$ and $\overline{\sigma^2}$ according to Eq. (15). To this end we fix the threshold b such that the value $\overline{A}=1$ is reached when the distance to the *Daphnia* is 1 cm which yields the value $b = 125/8$ μV. This means the suprathreshold region coincides with the region where the dipole approximation ($d \ll r$) loses significance. In this way we find $\overline{A}(r)$ and $\overline{\sigma}(R,\Lambda,N)$ which we can plug into the expression for the rates (16) and (17). These are used to compute asymptotic $\langle\dot{\varphi}\rangle$ and $\mathcal{D}$ which themselves are inserted into Eq. (7), eventually yielding $\langle n_{\mathrm{lock}}\rangle(r,R,\Lambda,N)$.

Before evaluating our analytic formulas numerically we have to mention a problem that arises from the fitted values for τ_1 and τ_2 [cf. Sec. III]. As is obvious from Eqs. (16) and (17) the maximal rate (occurring for $\overline{\sigma} \to \infty$) is given by $[2\pi\sqrt{\tau_1\tau_2}]^{-1}$ Hz. With $\tau_1=0.13$ s and $\tau_2=0.017$ s we thus find that $a_{1/2} \leqslant 3.4$ Hz which means the detecting unit switches much too slowly. However, since detecting sites are spread across the rostrum in abundance we may assume that the effective switching rate is much higher. Hence we scale up the prefactor of both rates until the expected effect becomes visible.

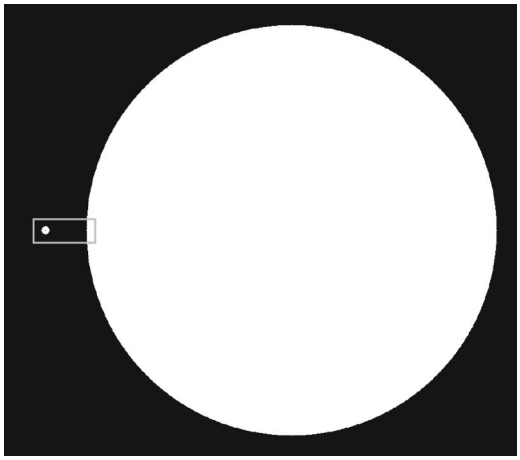

FIG. 12. The *Daphnia* swarm with a diameter of 100 cm (big white sphere) and the single *Daphnia* centered in the small white spot on a black background indicating the nondetectable region. The gray rectangle contains the region zoomed in Fig. 13.

VII. RESULTS

We visualize the results in the following way: We place the single *Daphnia* in the origin of our coordinate system and fix the center of the *Daphnia* cloud along the x axis at the position $(L,0,0)$; a suitable translation and three rotations will always render this setup possible. Then each triple (x,y,z) determines a position of the predator relative to the prey, i.e., $r=\sqrt{x^2+y^2+z^2}$ and the distance between the center of the *Daphnia* swarm and the detector R is $\sqrt{(x-L)^2+y^2+z^2}$.

For the swarm diameter we assume a value $\Lambda = 100$ cm; together with the density of 1000–9000 per liter mentioned in Sec. II we infer a number of up to $N = 5\,000\,000$ *Daphnia* clumping in the swarm. With these numbers at hand we can compute the value $\langle n_{\mathrm{lock}}\rangle$ for each position of the predator relative to the static prey and the static swarm.

To give the reader a realistic impression of the geometric dimensions we depict the swarm (big white ball) and the single *Daphnia* (in the center of the little white spot) on a black background, indicating the nondetectable region, in Fig. 12.

The gray rectangle contains the region relevant for SR. We zoomed this region and display our final result in the sequence of images in Fig. 13.

The sequence shows the spatial distribution of the quantity $\langle n_{\mathrm{lock}}\rangle$ with gray scale coding values (cf. the gray value bar). The single *Daphnia* is indicated by the little black spot inside the white sphere. The latter describes the region of

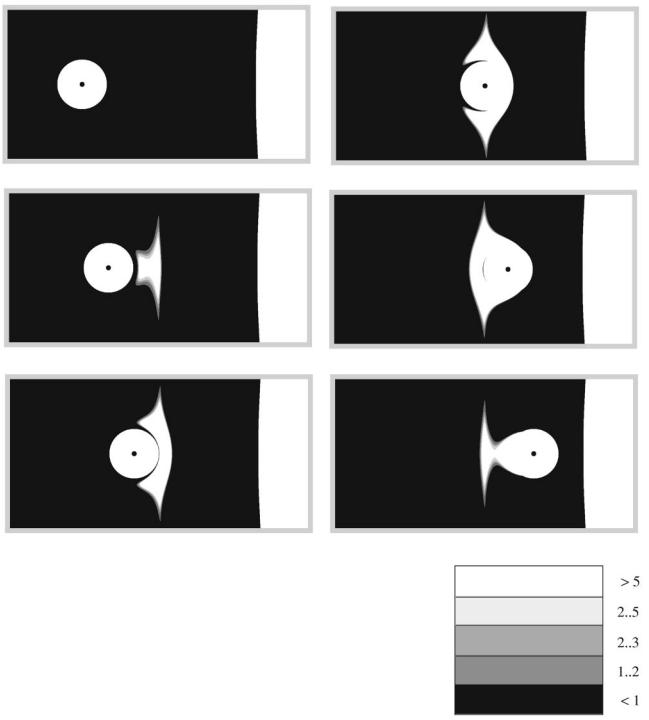

FIG. 13. The sequence of images shows the spatial distribution of the quantity $\langle n_{\mathrm{lock}} \rangle$ with values coded by gray values (cf. the gray value bar). The white region around the single *Daphnia* (black central spot) codes the suprathreshold signal region which also violates the dipole approximation; in this region the predator can detect the prey even in the absence of swarm noise. At intermediate distances (≈ 5 cm) to the swarm the single *Daphnia* has to dive through a ''firewall'' established by the optimal noise condition. As expected, the geometry of contour lines reflects the compromise between spheres around the single *Daphnia* and contour lines of noise intensity spreading concentrically around the swarm boundary.

suprathreshold signals, i.e., places were the fish can detect the *Daphnia* even in the absence of swarm noise. Moreover, within the white circle the dipole approximation loses significance. The depicted rectangle extends from 10 cm left of the swarm boundary up to 2 cm inside and over 6 cm in the vertical direction. From Fig. 13 we see that the single *Daphnia* has to dive through a ''firewall:'' Optimal noise widens the detection area beyond the initial white circle.

VIII. SUMMARY AND OUTLOOK

We have resumed the idea, first expressed by Russell *et al.* [1], that a nearby swarm of *Daphnia* provides a natural source of electric noise essential for the mechanism of SR. We modeled the swarm noise as OU noise generated by incoherent *Daphnia* activity. The rapid geometric decay of the noise intensity $D(R)$ and of the dipole signal amplitude $A(r)$ (near-field limit) restricts the spatial region of SR to a narrow band around the swarm boundary.

The quantity we used to measure noise-induced widening of the detection area was the mean duration of locking episodes [15] normalized to the period $2\pi/\Omega$ of the input signal. The description of (1:1) noise-induced phase locking is based on the phase difference φ between a dichotomic detector (predator) and a two-state, i.e., preprocessed harmonic input signal (prey). We employed analytic expressions for the average frequency $\langle \dot{\varphi} \rangle$ and the phase diffusion coefficient $\mathcal{D}$ derived in [14]. These are based on two rates a_1 and a_2 which, in this work, we adopted from [36] and which were derived for a threshold system driven by OU noise.

Most of the free model parameters were fitted to existing experimental data. The maximum flipping rate of the two-state detector was scaled up to render a pronounced effect; this tuning may be justified by accounting for cooperative effects of many detecting sites spread across the rostrum in abundance. Numeric evaluation of our analytic formulas supports the notion of noise-enhanced detectability quantitatively: At a certain distance the swarm builds a ''firewall'' which widens the detection area around a single *Daphnia* during its ''passage.''

Synchronization of noisy electrosensitive cells in the rostrum of a paddlefish with an externally applied electric signal was shown in an experiment [16]. For a 5 Hz stimulus a 1:17 locking mode was observed. Extension of our analysis beyond the assumed 1:1 locking mode requires further analytical work. An improved understanding of cooperative information processing done by many detecting sites in the rostrum and a better estimation of time constants and parameters would be desirable for planning a behavioral experiment designed to test the predicted effect.

ACKNOWLEDGMENTS

This work was supported by the Office of Naval Research, Physics Division and by the DFG in the framework of the Sfb555.

[1] D. Russell, L. Wilkens, and F. Moss, Nature (London) **402**, 291 (1999).
[2] L. Grande and W.E. Bemis, J. Vert. Paleontol. **11** (Memoir 1), 1 (1991).
[3] F. Jaramillo, and K. Wiesenfeld, Nature-neuroscience **1**, 384 (1998).
[4] L.A. Wilkens, D.F. Russell, X. Pei, and C. Gurgens, Proc. R. Soc. London **264**, 1723 (1997).
[5] P.E. Greenwood, L.M. Ward, D.F. Russell, A. Neiman, and F. Moss, Phys. Rev. Lett. **84**, 4773 (2000).
[6] R. Benzi, S. Sutera, and A. Vulpiani, J. Phys. A **14**, L453 (1981); C. Nicolis, Tellus **34**, 1 (1982); R. Benzi, G. Parisi, S. Sutera, and A. Vulpiani, *ibid.* **34**, 10 (1982).
[7] J.K. Douglass, L. Wilkens, E. Pantazelou, and F. Moss, Nature (London) **365**, 337 (1993); J.E. Levin and J.P. Miller, *ibid.* **380**, 165 (1996).
[8] S.M. Bezrukov, and I. Vodyanoy, Nature (London) **378**, 362 (1995).
[9] K. Wiesenfeld and F. Moss, Nature (London) **373**, 33 (1995).
[10] F. Moss, in *Contemporary Problems in Statistical Physics*, edited by G.H. Weiss (SIAM, Philadelphia, 1994), pp. 205–253; F. Moss, D. Pierson, and D. O'Gorman, Int. J. Bifurcation Chaos Appl. Sci. Eng. **6**, 1383 (1994); V. Anishchenko, F. Moss, A. Neiman, and L. Schimansky-Geier, Sov. Phys. Usp.

42, 7 (1999); F. Moss, in *Self-Organized Biological Dynamics & Nonlinear Control*, edited by J. Walleczek (Cambridge University Press, Cambridge, England, 2000), p. 236; L. Gammaitoni, P. Hänggi, P. Jung, and F. Marchesoni, Rev. Mod. Phys. **70**, 223 (1998).

[11] Z. Gingl, L.B. Kiss, and F. Moss, Europhys. Lett. **29**, 191 (1995); S.M. Bezrukov, and I. Vodyanoy, Nature (London) **385**, 319 (1997).

[12] B. McNamara and K. Wiesenfeld, Phys. Rev. A **39**, 4854 (1989).

[13] A. Longtin, A. Bulsara, and F. Moss, Phys. Rev. Lett. **67**, 656 (1991).

[14] J.A. Freund, A. Neiman, and L. Schimansky-Geier, Europhys. Lett. **50**, 8 (2000).

[15] J.A. Freund, A. Neiman, and L. Schimansky-Geier, *Stochastic Climate Models. Progress in Probability*, edited by P. Imkeller and J. von Storch (Birkhaeuser, Boston, 2001).

[16] A. Neiman, X. Pei, D. Russell, W. Wojtenek, L. Wilkens, F. Moss, H. Braun, M. Huber, and K. Voigt, Phys. Rev. Lett. **82**, 660 (1999).

[17] X. Pei, L. Wilkens, and F. Moss, Phys. Rev. Lett. **77**, 4679 (1996).

[18] A. Neiman, F. Moss, L. Schimansky-Geier, and W. Ebeling, in *Applied Nonlinear Dynamics and Stochastic Systems Near the Millennium*, edited by J.B. Kadtke and A. Bulsara (AIP, Woodbury, 1997), pp. 151.

[19] S. Young and C. Getty, Anim. Behav. **35**, 541 (1987); K.M. Cuddington and E. McCauley, Can. J. Zool. **72**, 1217 (1994).

[20] K.H. Jensen, P.J. Jakobsen, and O.T. Kleiven, Hydrobiologia **368**, 123 (1998).

[21] J. Ringelberg, Memorie Dell'Istituto Italiano di Idrobiologia **45**, 285 (1987).

[22] Z. Brandl and C.H. Fernando, Can. J. Zool. **49**, 775 (1971); J.M. Colebrook, J. Anim. Ecol. **29**, 243 (1960).

[23] O.V. Kvam and O.T. Kleiven, Hydrobiologia **307**, 177 (1995); J. Davies, Hydrobiologia **120**, 103 (1985).

[24] M. Galle, R. Neurohr, G. Altmann, F.A. Popp, and W. Nagl, Experientia **47**, 457 (1991).

[25] S. Young, P.J. Watt, J.P. Grover, and D. Thomas, J. Anim. Ecol. **63**, 611 (1994).

[26] P.J. Jakobsen and G.H. Johnsen, Anim. Behav. **36**, 991 (1988).

[27] P.J. Jakobsen and G.H. Johnsen, Anim. Behav. **36**, 986 (1988).

[28] J. Pijanowska and A. Kowalczewski, Freshwater Biol. **37**, 649 (1997).

[29] W. Wojtenek, X. Pei, and L. Wilkens (unpublished).

[30] G.E. Uhlenbeck and L.S. Ornstein, Phys. Rev. **36**, 823 (1930); P. Jung, Phys. Rev. E **50**, 2513 (1994); K. Dolan, A. Witt, M.L. Spano, A. Neiman, and F. Moss, *ibid.* **59**, 5235 (1999).

[31] R.L. Stratonovich, *Theory of Random Noise*, Vols. I and II (Gordon and Breach, New York, 1964).

[32] J.J. Hesse and L. Schimansky-Geier, Z. Phys. B: Condens. Matter **84**, 467 (1991).

[33] I.I. Blekhman, *Synchronization in Science and Technology* (Nauka, Moscow, 1981, in Russian, English translation: ASME Press, New York, 1988); P. Landa, *Nonlinear Oscillations and Waves in Dynamical Systems* (Kluwer Academic, Dordrecht, 1996).

[34] R. Adler, Proc. IRE **34**, 351 (1946); P. Hänggi and P. Riseborough, Am. J. Phys. **51**, 347 (1983).

[35] A. Neiman, A. Silchenko, V. Anishchenko, and L. Schimansky-Geier, Phys. Rev. E **58**, 7118 (1998).

[36] P. Jung, Phys. Lett. A **207**, 93 (1995).

[37] A. Neiman, L. Schimansky-Geier, F. Moss, B. Shulgin, and J.J. Collins, Phys. Rev. E **60**, 284 (1999).

[38] N.G. Van Kampen, *Stochastic Processes in Physics and Chemistry* (North-Holland, Amsterdam, 1992).